2022

The Current Hunt for Nitric Oxide's Effects on the *Homarus americanus* Cardiac Ganglion

Joanna Lin
Bowdoin College

The Current Hunt for Nitric Oxide's Effects on the *Homarus americanus* Cardiac Ganglion

An Honors Paper for the Program of Neuroscience

By Joanna Lin

Bowdoin College, 2022

Table of Contents

Table of Figures

Acknowledgements

Over the course of my time at Bowdoin, I have been incredibly fortunate to learn and collaborate with many extraordinary scientists. This project could not have been completed without the encouragement and mentorship of my advisor, Patsy Dickinson. I owe my deepest thanks to Patsy for her dedication to research and teaching. It has been an honor to learn from you, Patsy, both in the classroom and the laboratory. You are inspiring to everyone who knows you, and I hope to continue your legacy of uplifting other scientists. I also want to thank all the Bowdoin Neuroscience faculty members, especially my thesis reviewers, Jennifer Honeycutt and Manuel Diaz-Rios, for their thoughtful and continual support throughout my Bowdoin neuroscience education.

Many students have been fortunate to be a part of the Dickinson Lab, and I must thank the past members for establishing the foundations of our research and the present ones for continuing the work. Thank you, Dan, Anthony, Josie, Justin, Isabel, Hannah, and Emily, for your support over the summer and school year. As we teach one another and pass on the knowledge we have gained, I am truly proud to be a part of the Dickinson research network that spans many years.

Outside of the Neuroscience Program, I also want to acknowledge Professor Kana Takematsu, Beth Stemmler, and Danielle Dube for always offering their support and advice in navigating research as women in STEM. Their kindness and intentionality bring compassion into Druckenmiller, welcoming students from all types of backgrounds into the sciences with open arms. Thank you all for providing wonderful examples of how to shape the systems we live in to make them equitable and just for those who come after us.

Finally, I want to thank my family and friends who have supported me throughout my research. To my family, I would not be where I am today without your support and encouragement. Thank you for listening to me endlessly talk about lobsters. To Grace and Alissa, thank you both for your friendship and chaotic (good) energies. To Prith, Tang, Tugi, Justin, and Pat, thank you all for keeping me focused on the big picture. And to Griffin, you are my sunshine on the rainiest of days. Thank you for believing in me even in the moments when I do not.

This research project was supported by the Bowdoin College Program of Neuroscience, the Alan and Marsha Paller Neuroscience Research Fellowship, the Maine Space Grant Consortium, the NIH Maine INBRE grant, and the NSF Grant.

Abstract

The crustacean heartbeat is produced and modulated by the cardiac ganglion (CG), a central pattern generator. In the American lobster, *Homarus americanus*, the CG consists of 4 small premotor cells (SCs) that electrically and chemically synapse onto 5 large motor cells (LCs). Rhythmic driver potentials in the SCs generate bursting in the LCs, which elicit downstream cardiac muscle contractions that are essential for physiological functions.

Endogenous neuromodulators mediate changes in the CG to meet homeostatic demands caused by environmental stressors. Nitric oxide (NO), a gaseous neuromodulator, inhibits the lobster CG. Heart contractions release NO, which directly decreases the CG burst frequency and indirectly decreases the heartbeat amplitude, to mediate negative feedback. I investigated NO's inhibitory effects on the CG to further understand the mechanisms underlying intrinsic feedback.

Using extracellular recordings, I examined NO modulation of the SCs and LCs when coupled in the intact circuit and when firing independently in the ligatured preparation. Using two-electrode voltage clamp, I additionally analyzed the modulation of channel kinetics. Based on previous studies, I hypothesized that NO decreases the burst frequency of the LCs and SCs by modulating conductance properties of the voltage-gated A-type potassium current (I_A). My data showed that NO decreased the burst frequency in the LCs and the burst duration in the SCs in a state-dependent manner. Furthermore, NO increased the I_A inactivation time constant to decrease the LCs' burst frequency. Thus, NO mediated inhibitory effects on cardiac output by differentially targeting both cell types and altering the I_A current kinetics.

1. Introduction

A robust and rhythmic heartbeat that is critical for a healthy cardiovascular system underlies the survival of animals. The neurogenic heartbeat in crustaceans is driven and maintained by a central pattern generator (CPG), a neural circuit that produces rhythmic patterned movements independently of sensory information or higher centers of neural control (Dickinson, 2006; Marder & Bucher, 2001). In the *Homarus americanus* (lobster) heart, the cardiac ganglion (CG) is a simple CPG network that consists of 9 electrically and chemically coupled neurons: 4 small premotor cells (SCs) that synapse onto 5 large motor cells (LCs; Hartline, 1979; Cooke, 2002). By understanding the conductance properties within the invertebrate *Homarus* CG model, we can gain insight into conserved yet more complex mechanisms within vertebrate nervous systems (Hooper & DiCaprio, 2004).

On the inner dorsal wall of the heart, the *Homarus* CG forms a branching trunk critical for inducing heart contractions (Fig. 1A). The SCs fire rhythmically without input and act as a pacemaker by initiating bursting in the LCs (Cooke, 2002). The LCs are motor neurons that innervate and activate the heart muscle to contract while transmitting signals to SCs through feedback mechanisms (Berlind, 1989). While there is putative diversity between innexins of different cell types (Christie et al., 2020), the gap junctions between the LCs send signals to one another but act as low-pass filters and do not transmit rapid spikes (Hartline, 1979). Electrical synapses within and between the cell types enable them to fire in synchrony (Fig. 1B), with bursts that begin with a high spike firing frequency that eventually slows within the burst (Hartline, 1967).

The bursting pattern of the LCs primarily relies on signals from the SCs; however, each cell type can fire independently. Tightening a suture silk ligature anterior to LC4 blocks electrical

and chemical signaling between the cell types, demonstrated by the unsynchronized bursting of the LCs and SCs (Oleisky et al., 2020). In *Homarus* LCs, depolarization to a threshold of approximately -45 mV induces bursting up to 20 mV above resting potential (Cooke, 2002). Driver potentials (DPs) are intrinsic, slow, regenerative depolarizations lasting 200 ms or longer that drive these bursts of action potentials in response to gradual pacemaker potentials or excitatory synaptic potentials (Fig. 1C; Tazaki & Cooke, 1986). When depolarized, the DPs have a characteristic plateau shape that slowly declines and ends with a rapid hyperpolarization.

The waveform of DPs is dictated primarily by four currents: voltage-gated calcium (I_{Ca}), delayed rectifier potassium (I_{Kd}), calcium-dependent potassium (I_{KCa}), and a transient, voltage-gated A-type potassium (I_A; Hooper & DiCaprio, 2004; Tazaki & Cooke, 1986, 1990). Depolarization to a threshold of approximately -45 mV activates I_{Ca}, which generates the DP in both LCs and SCs (Cooke, 2002). Once I_{Ca} activates, a depolarization of approximately 20 mV occurs until the channel inactivates and the potassium channels activate. After I_{Kd} and I_{KCa} channels are activated, the cell becomes hyperpolarized. The hyperpolarization during the refractory phase de-inactivates I_A channels, which increases the latency of the following burst (Fig. 1D). The conductance properties of these ionic currents, including the time- and voltage-dependence of activation and inactivation, underlie the intrinsic bursting patterns of both the LCs and SCs of the *Homarus* CG (Marder and Calabrese, 1996).

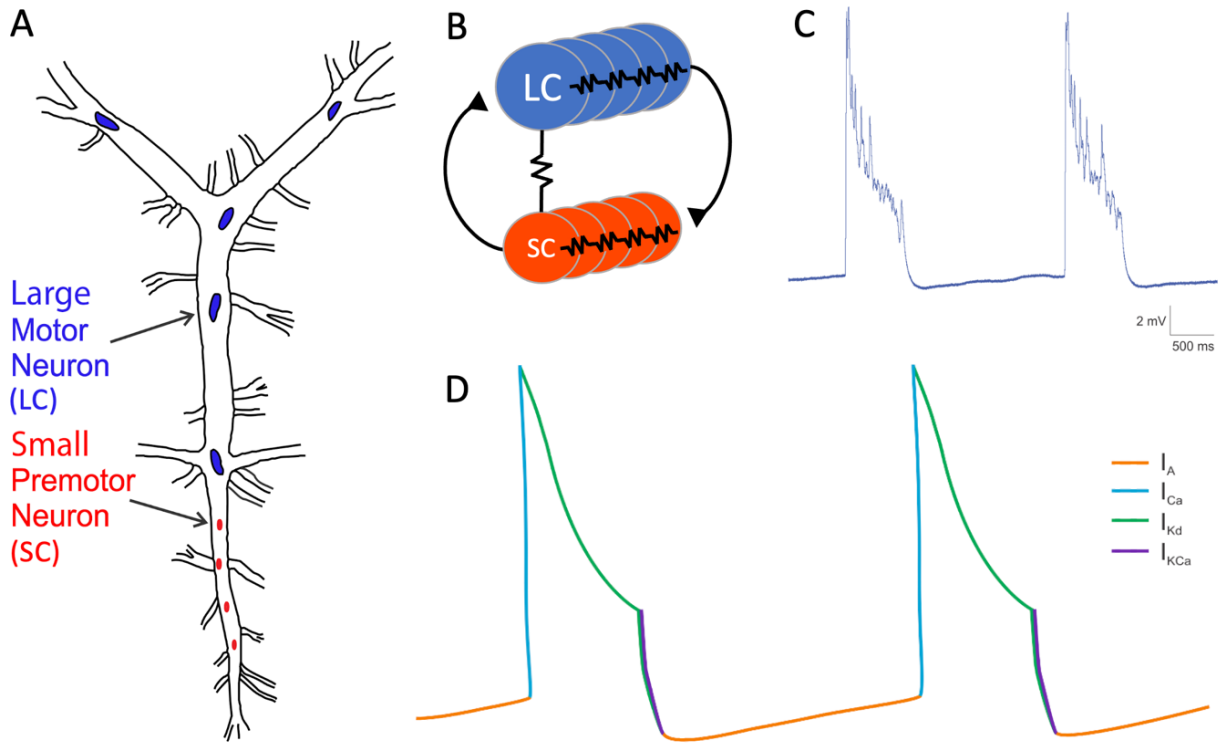

Figure 1. Electrophysiology of the *Homarus americanus* cardiac ganglion (CG). *(A)* The cardiac ganglion contains 4 small premotor cells (SCs) and 5 large motor cells (LCs). The SCs (red) drive bursting in the LCs, which elicit downstream heart muscle contractions. *(B)* The 5 LCs and 4 SCs are electrically and chemically coupled for synchronized rhythmicity. *(C)* Intrinsic driver potentials (DPs) in the LCs and SCs drive bursts of action potentials. The resting membrane potential is approximately -55 mV. *(D)* Several currents shape the waveform of the DPs, such as the voltage-gated A-type potassium current (I_A), voltage-gated calcium current (I_{Ca}), delayed rectifier potassium current (I_{Kd}), and calcium-dependent potassium current (I_{KCa}).

Endogenous neuromodulators such as nitric oxide (NO) induce appropriate changes in the CG (Cooke, 2002; Mahadevan, 2004). NO is a gaseous and versatile neuromodulator that has been highly conserved across invertebrates, vertebrates, and the broader metazoan and protozoan kingdom (Torreilles, 2001). In humans, NO is best known as a vasodilator in blood pressure regulation (Cyr et al., 2020). Additionally, NO is involved in numerous other pathways: metabolic regulation (Tenopoulou & Doulias, 2020), neurodegeneration of the central nervous system (Tse,

2017), carcinogenesis in colon cells (Oláh et al., 2018), sleep deprivation (Yamakawa et al., 2018), and cardioprotection (Klinger & Kadowitz, 2017; Totzeck et al., 2017; Zhang, 2017).

In the *Homarus* cardiac musculature and ganglion, NO mediates negative feedback (Mahadevan, 2004). When the heart musculature contracts, it releases the endogenous NO synthesized in the cardiac muscle, which diffuses to the CG and decreases the burst frequency by approximately 20% (Fig. 2; Mahadevan, 2004). Since the lobster heart is neurogenic, the inhibited CG bursting frequency consequently decreases the burst frequency of heart contractions. The heartbeat amplitude also decreases as an indirect result of the decreased CG burst frequency, mediated by the resultant decrease in synaptic facilitation between the CG and muscle fibers (Mahadevan, 2004).

However, the physiological mechanisms by which NO decreases the burst frequency of the CG have yet to be determined. Previous research suggests that NO activates a signaling cascade that increases cGMP metabolism in crustaceans (Scholz et al., 2002), but the specific voltage-gated currents that mediate the inhibition of bursting are still unknown. Unpublished computational modeling research from the Dickinson Lab demonstrated that an increase in the maximal conductance of I_A mimicked the endogenous inhibitory effects of NO on burst frequency in the *Homarus* CG. An increased I_A current would further hyperpolarize the cell membrane potential and slow the depolarization to threshold (Tazaki & Cooke, 1986; Cooke, 2002). Consequently, the burst frequency and cycle period would be decreased without directly altering the burst duration.

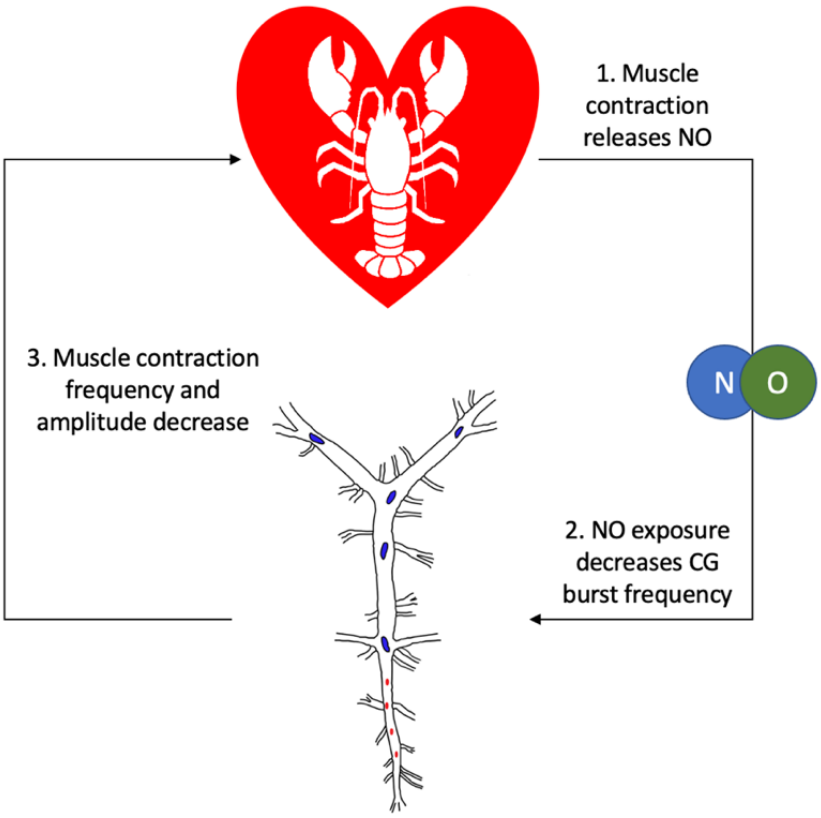

Figure 2. Nitric oxide modulation of the *Homarus* CG. Muscle contractions release endogenously produced NO, which diffuses to the CG and subsequently decreases the burst frequency. Since the lobster heart is neurogenic, the inhibited CG bursting leads to a decreased frequency and amplitude of the heart contractions. The mechanism by which NO decreases the CG burst frequency is not well-characterized.

In this thesis, I investigated the inhibitory effects of NO in the *Homarus* CG to elucidate possible conserved mechanisms that provide flexibility in patterned movements. Through extracellular and intracellular two-electrode voltage clamp (TEVC) recordings, I explored (1) differential NO effects on bursting patterns between the LCs and SCs, and (2) intracellular conductance properties that may mediate inhibited bursting patterns. Based on previous literature, I hypothesized that the LCs and SCs will decrease in burst frequency and duty cycle during NO

exposure to yield the identified decreased cardiac muscle output. Additionally, I hypothesized that the inhibition is mediated through an increased I_A current that prolongs the interburst interval.

My data demonstrate that NO increased the burst duration and decreased the burst frequency and duty cycle of both the LCs and SCs in the intact CG. When the cells were decoupled, NO decreased the burst frequency in the LCs and the burst duration in the SCs. These results suggest that NO acts on both the LCs and SCs to inhibit the CG bursting activity, but NO alters different bursting parameters. Interestingly, the effects of NO on burst frequency and duration were also state-dependent. Furthermore, NO mediated its inhibitory effects by modulating the time-dependence of inactivation for I_A. Thus, these findings suggest NO inhibits cardiac output by targeting both cell types of the CG and altering outward current kinetics. Given the abundance of NO across species, this mechanism may be highly conserved or have analogous mechanisms that sustain patterned movements.

2. Methods

2.1 Animals

American lobsters (*Homarus americanus*) were purchased from seafood stores in Brunswick, Maine, USA. Lobsters fed with shrimp or squid weekly were kept in recirculating natural seawater aquaria (10-12°C) with 12:12 hour light-dark cycles. Only preparations that maintained stable, rhythmic bursting or a steady voltage clamp were included in the sample for extracellular recordings (n=10 successful/15 total animals) or intracellular recordings (n=4 successful/30 total animals), respectively.

2.2 CG Isolation

After anesthetizing lobsters in ice for 30 minutes, the heart was dissected from the cephalothoracic carapace in chilled (8-10°C) physiological saline with a pH of 7.45 (composition in mM: 479.12 NaCl, 12.74 KCl, 13.67 $CaCl_2$, 20.00 $MgSO_4$, 3.91 Na_2SO_4, 11.45 Trizma base, and 4.82 maleic acid; Dickinson et al., 2018). The CG was then isolated by ventrally cutting the heart and dissecting the main ganglion trunk and branches from the surrounding muscle.

2.3 SNAP Preparation

The NO donor S-nitroso-N-acetyl-penicillamine (SNAP; Sigma-Aldrich) was perfused with saline at a concentration of 10^{-5} M across preparations for 10-15 minutes, followed by a 30–45-minute saline wash (Mahadevan, 2004). The wash ensured that the preparation remained sensitive to NO modulation and that the effects of NO were reversible. The inhibitory effects of SNAP are concentration dependent and fit a Michaelis-Menten equation with an IC_{50} of 5×10^{-6} M (Mahadevan, 2004). It has been shown that bath application of 10^{-5} M SNAP decreases the burst

frequency of the CG in the intact *Homarus* heart, which can be reversed with a saline wash (Mahadevan, 2004). A preparation was included in the sample if NO induced a minimum decrease of 10% decrease in burst frequency. Stock solutions of SNAP (10^{-3} M) in physiological saline were stored at -20°C for up to 5 weeks to prevent degradation.

2.4 Extracellular Experiments

2.4.1 Extracellular Setup

After the CG was pinned to a Sylgard 184-lined petri dish (Dow Corning, Midland, MI, USA), petroleum jelly wells were made around the anterolateral nerve (ALN) distal to LC 1 and around the trunk between LC 4 and 5 to record the burst activity of LCs and SCs, respectively (Fig. 3). Two pairs of stainless-steel electrodes were used to record activity, with one electrode placed in the well and another in the bath. Temperature was held between 10°C and 12°C by a Peltier cooling unit (CL-100 bipolar temperature controller and SC-20 solution heater/cooler; Warner Instruments, Hamden, CT) and temperature probe (Warner Instruments, Hamden, CT), while physiological saline was perfused (5 mL/min) across the CG via a Rabbit peristaltic pump (Gilson, Middleton, WI). A single strand of 6-0 suture silk fiber was loosely tied around the CG trunk anterior to LC 4 (Fig. 3). Tightening this ligature decoupled the LCs and SCs, leading to independent bursting recordings of the LCs from the ALN and SCs from the trunk (Oleisky et al., 2020).

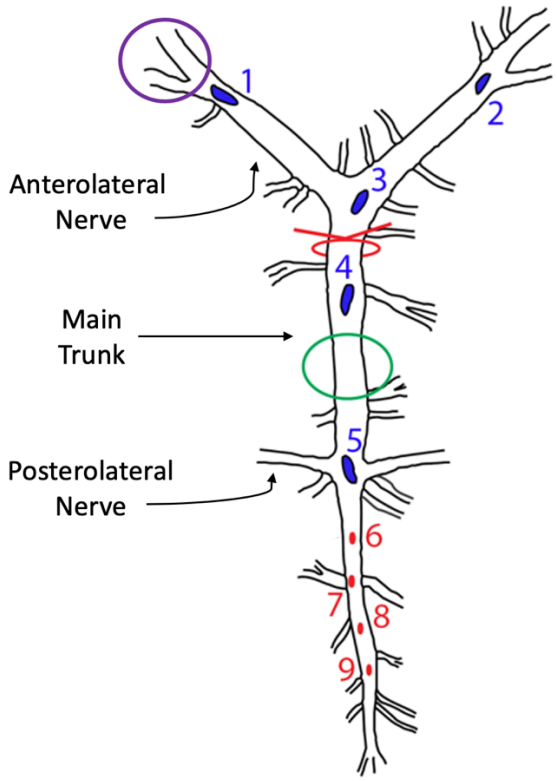

Figure 3. Extracellular setup of intact and ligatured CG preparations. A ligature (red) placed anterior to LC 4 decoupled the LCs (blue) and SCs (red) for individual bursting recordings. The circled purple and green ovals indicate extracellular recording sites for the LCs in the anterolateral nerve and SCs in the trunk, respectively.

2.4.2 Extracellular Recordings

Once the CG established a stable, consistent firing pattern, the bursting activity was recorded from the ALN and trunk for 10 minutes. Following the control recording, NO was administered, and the CG was recorded for an additional 10-15 minutes. Afterwards, the CG was washed with the saline solution for 30-45 minutes. Once the effects of NO had washed out, the CG was ligatured immediately anterior to LC 4 and allowed to re-establish a stable firing pattern (~1 hour; Oleisky et al., 2020). When the bursting pattern was stable, the NO application protocol was repeated to determine how NO independently affected the LCs and SCs.

2.5 Intracellular Two-Electrode Voltage Clamp (TEVC)

2.5.1 TEVC Setup

After the whole heart was dissected from the lobster, the CG was isolated and pinned to a Sylgard 184-lined petri dish. The ganglionic sheath overlying LC1 and LC2 was cut and pinned aside to expose the cell bodies, so they could be penetrated with microelectrodes. To voltage clamp the CG, two glass microelectrodes filled with squid cytoplasmic fluid (Hooper et al., 2015) and having resistances of ~15 MΩ were inserted into LC1 or LC2 to record the ionic currents flowing across the cell membrane. To isolate the outward currents, the CG was perfused with tetrodotoxin (TTX; 10^{-7} M; 5.0 ml/min) dissolved in physiological saline until the sodium currents were blocked.

2.5.2 TEVC Recordings

The maximum I_A current ("peak current") was measured as the difference between the peak outward current after maximal deinactivation of I_A channels and the residual leak currents measured at steady state. To deinactivate the I_A channels, cells held at a -70 mV holding potential underwent a pre-pulse step to -90 mV for 2 seconds (Fig. 4A). Following the pre-pulse, cells were immediately clamped to potentials between -40 and +20 mV for 2 seconds in 10 mV increments and then returned to -70 mV. The TEVC protocol was run three times in each cell with an intermittent 60 second rest in both the control and SNAP conditions to determine how the peak I_A current and time constant of inactivation were modulated by NO.

2.6 Data Acquisition

Extracellular signals were amplified with a differential AC amplifier (1700 A-M Systems; Sequim, WA), while intracellular signals were amplified using an Axoclamp 2-B amplifier (Axon

Instruments). Signals were digitized at 10 kHZ with a Micro 1401 digitizer (Cambridge Electronic Design (CED), UK) and recorded using Spike2 (v.7.17; CED). Extracellular recordings were analyzed with functions in Spike 2 and scripts written by Dr. Dirk Bucher. Action potentials ("spikes") were defined as peaks with a minimum interval of 0.001 s and a minimum amplitude of approximately 0.01 mV for SCs and 0.15 mV for LCs (Oleisky et al., 2020). A burst was defined as a trail of at least 5 spikes occurring at a frequency of at least 100 Hz (Oleisky et al., 2020). Burst frequency (Hz), burst duration (s), and duty cycle were quantified for the LCs and SCs in intact and ligatured CG preparations. Burst duration was calculated as the time between the first and last spike in a burst. Duty cycle was calculated as the burst duration divided by the cycle period, a measurement defined as the total time between the first spike of a burst and the following burst.

For intracellular signals, I analyzed the peak outward current, the peak I_A current, and the time constant of I_A inactivation. The peak outward current was determined using "Find Peak" in Spike 2 (Fig. 4B). The peak I_A current was calculated as the difference between the peak outward current and the steady state, the mean of a 1.0 s interval that was 0.5 s following the peak that accounted for leak and outward currents other than the I_A current. The time constant of I_A inactivation was determined using the "Exponential Fit" function in Spike 2 for a 0.2 s interval that was 0.1 s after the peak on the -20 mV step, which consistently demonstrated a clear steady state and peak across preparations. The interval was selected temporarily after the peak to record I_A inactivation without the variable effects of the voltage clamp.

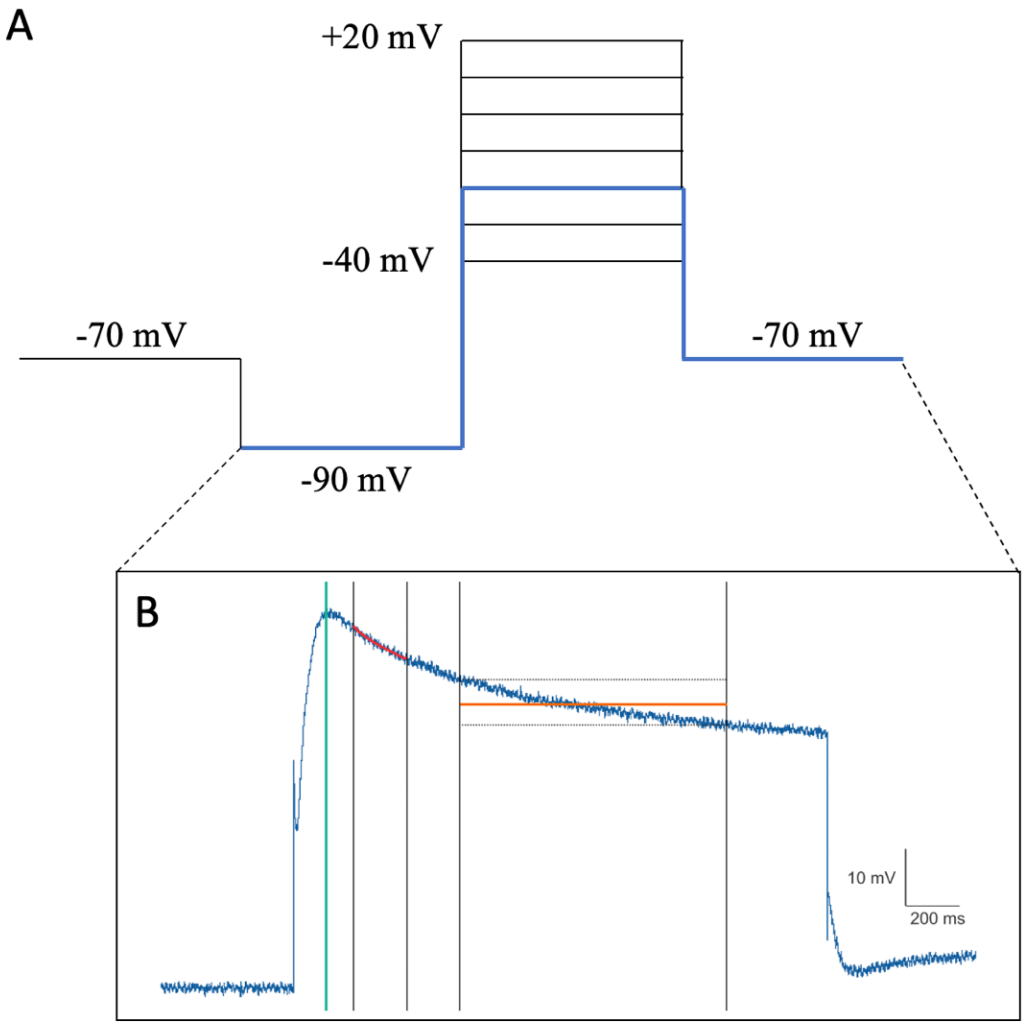

Figure 4. Intracellular Two-Electrode Voltage Clamp (TEVC) Protocol and Analysis. *(A)* Voltage step protocol used to maximize I_A current. Cells held at -70 mV first underwent a pre-pulse step to -90 mV, then they were clamped to voltage steps between -40 and +20 mV in 10 mV increments. Each step was held for 2 seconds. The protocol was run 3 times in each cell and condition, with 60 seconds between each run. *(B)* Image inset demonstrates data analysis of current trace during a voltage step to -20 mV step (blue). The peak outward current was measured using Spike2 "Find Peak" (green line). The peak I_A current was calculated as the difference between the peak outward current and the steady state, the mean of a 1.0 s interval that was 0.5 s following the peak to account for other leak and outward currents (orange). The time constant of inactivation for I_A was calculated using an exponential fit function in a 0.2 s interval that was 0.1 s after the peak on the -20 mV step each run (red).

2.7 Statistical Analysis

After data were sorted in Microsoft Excel (v.16.54), an Excel macro extracted and averaged 50 bursts in the control, SNAP, and wash conditions when bursting activity was constant. Statistical analyses were then run using Prism 9 (GraphPad Software, v.9.0.1). One-way mixed ANOVAs were conducted to compare the bursting parameters of the LCs and SCs in the intact and ligatured preparation. Two-tailed paired t-tests analyzed the effects of SNAP on the extracellular bursting parameters and the intracellular time constant of inactivation. A two-way repeated measures ANOVA was run to explore the effects of SNAP on the peak outward current and peak I_A current. In all analyses, a post-hoc Bonferroni's multiple comparisons test was used to follow-up significant and trending main effects. For all experiments, data were considered significant when $p < 0.05$ and trending when $0.05 \leq p < 0.08$. All data are presented as mean ± SEM.

3. Results

This study investigated NO modulation within the intact and subsequently ligatured *Homarus americanus* CG to elucidate the underlying mechanisms of intrinsic negative feedback. I analyzed the burst frequency, burst duration, and duty cycle of the LCs and SCs to assess the effects of tying a ligature and applying SNAP, a NO donor. I also examined whether the effects of NO on the LCs and SCs were state-dependent. After confirming NO modulation within the LCs, I used the intracellular TEVC technique to assess whether differences in the I_A voltage-dependence of activation and time constant of inactivation mediated the extracellular effects of NO.

3.1 Ligaturing the CG decoupled the LCs and SCs.

To explore the independent effects of NO on the bursting patterns of the LCs and SCs, I tightened a ligature around the CG to decouple the two cell types. While the bursting of the LCs and SCs were phase-locked in the intact preparations, the bursting patterns were no longer synchronized once the preparations were ligatured (Fig. 5A). Tying the ligature had significant effects on each of the three bursting parameters: (1) burst frequency, (2) burst duration, and (3) duty cycle ($p < 0.0001$, one-way mixed ANOVA for all parameters).

Comparing between intact and ligatured preparations, the burst frequency was significantly increased in both the LCs and SCs after tightening the ligature (post-hoc Bonferroni multiple comparisons test; $p = 0.0006$ for both cell types; Fig. 5B). The burst duration of the ligatured LCs was significantly decreased ($p = 0.0071$; Fig. 5C), but there were no significant differences in the SCs' burst duration ($p > 0.99$). Additionally, the duty cycles of both ligatured cell types were not significantly different from the duty cycle of intact preparations ($p > 0.99$; Fig. 5D).

Between the two cell types in the ligatured preparations, there were no significant differences in the burst frequency ($p > 0.99$; Fig. 5A). The burst duration was significantly shorter in LCs compared to SCs in the ligatured CGs ($p = 0.0006$; Fig. 5B). Additionally, the duty cycle of the SCs was significantly greater than the LCs in ligatured preparations ($p < 0.0001$; Fig. 5C). The duty cycle of both cell types in the ligatured preparations did not significantly differ from the duty cycle of the intact preparations, highlighting that the duty cycle of the two cell types deviated from the baseline in opposite manners. The cells were bursting asynchronously and effectively decoupled after tightening a ligature, making this method effective for comparing NO modulation of the LCs and SCs.

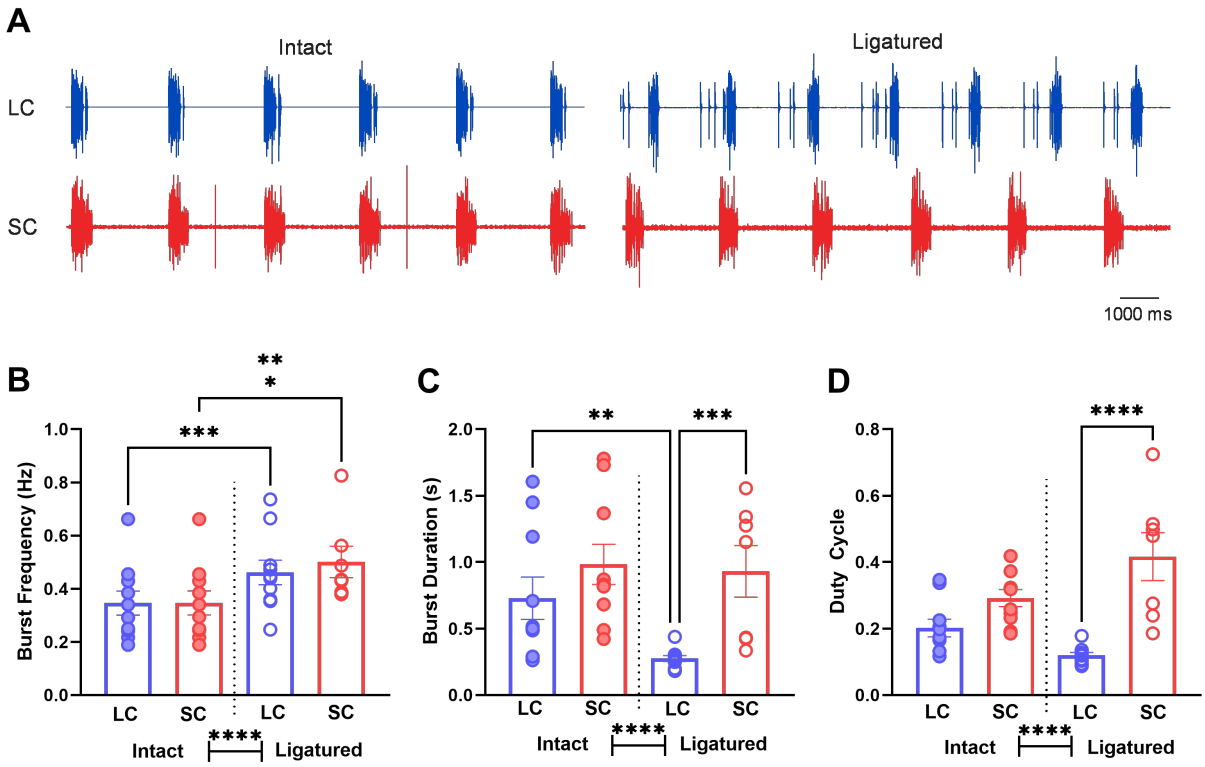

Figure 5. Tightening a ligature decoupled the large cells (LCs) and small cells (SCs) of the *Homarus* CG. *(A)* Representative raw traces of bursting activity in the intact and ligatured CG illustrated independent bursting patterns between the LCs (blue) and SCs (red) after tightening a ligature. A significant main effect on burst frequency, burst duration, and duty cycle was detected across the two cell types of the intact and ligatured CG, indicated by the bars between intact and ligatured text (one-way mixed ANOVA, $p < 0.0001$). *(B)* While there were no significant differences in the burst frequency between the ligatured cell types, the burst frequency significantly increased from the intact preparations in both the LCs and SCs ($p = 0.0006$ for both cell types). *(C)* Ligatured preparations had a significantly shorter burst duration in the LCs compared to intact preparations ($p = 0.0071$). Additionally, the LCs of ligatured preparations had a significantly shorter burst duration than the ligatured SCs ($p = 0.0006$). *(D)* In the ligatured CG, the duty cycle of SCs was significantly greater than the LCs ($p < 0.0001$), but not significantly different from the duty cycle of intact SCs. The duty cycle of the LCs was not significantly different between the intact and ligatured preparation. Statistical significance was determined using post-hoc Bonferroni tests. Data presented as mean ± SEM. The ligatured SCs condition had a sample size of n=7, while all other conditions had a n=10. ** = $p < 0.01$, *** = $p < 0.001$, **** = $p < 0.0001$.

3.2 NO elicited a decreased burst frequency and increased burst duration in the intact CG.

Since the LCs and SCs were coupled and fired in synchrony in the intact CG, the two cell types were similarly modulated by NO. Representative raw bursting traces of the LCs and SCs illustrated that SNAP drastically decreased the burst frequency of both cell types (Fig. 6A). Representative time-course graphs also demonstrated that SNAP decreased the burst frequency and duty cycle of both the intact LCs and SCs, while increasing the burst duration in both cell types (Fig. 6, B and C). The burst duration transiently increased above baseline when SNAP was being washed out, which may be an artifact of temperature changes and air bubbles when changing solutions.

Quantifying these changes to the bursting activity, SNAP significantly decreased the burst frequency of both the LCs and SCs (paired two-tailed t-tests; $p < 0.001$, n = 10 for both cell types; Fig. 7, A and B). In accordance with the time-course graphs, the burst duration was significantly increased by SNAP in the intact LCs and SCs (LCs: $p = 0.0335$, SCs: $p = 0.0364$, n = 10 for both cell types; Fig. 7, C and D). Despite the increase in burst duration, the duty cycle of the intact LCs and SCs was significantly decreased (LCs: $p = 0.0008$, n = 10; SCs: $p = 0.0004$, n = 10; Fig. 7, E and F). Thus, NO inhibits the intact CG by decreasing the frequency and increasing the duration of bursts, resulting in a decreased duty cycle of both cell types.

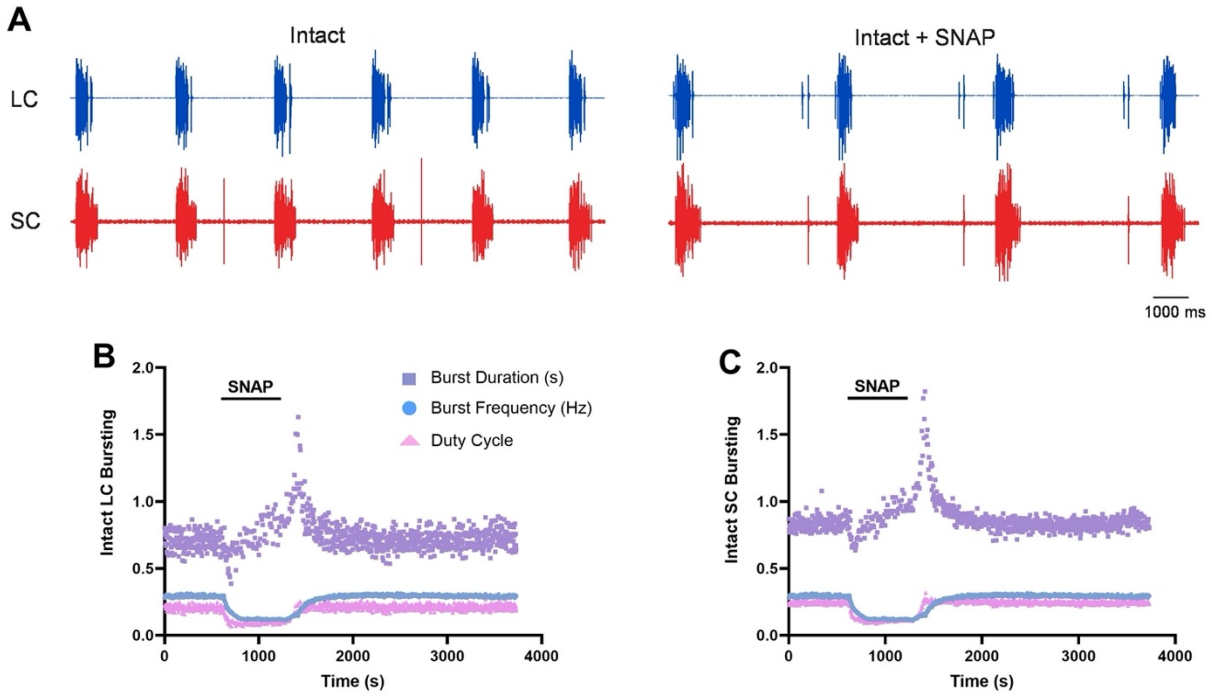

Figure 6. NO altered burst duration, burst frequency, and duty cycle in the intact CG. *(A)* Raw bursting traces of the SCs and LCs in a representative intact CG in the control and SNAP condition demonstrated a distinct decrease in bursting frequency and slight increase in burst duration when the cells were exposed to SNAP. *(B)* In the intact LCs, exposure to 10^{-5} M SNAP for 10 minutes (indicated by bar) decreased the burst frequency and duty cycle while increasing the burst duration. The burst duration in both populations transiently increased and decreased while transitioning between conditions, likely due to temperature changes or air bubbles. The acute exposure to SNAP also allowed for the effects to be washed out by saline (30-45 minutes). *(C)* The SCs were similarly affected by NO, with an increased burst duration and decreased burst frequency and duty cycle. The chemical and electrical coupling between the cells elicited synchronous bursting and parallel effects of NO.

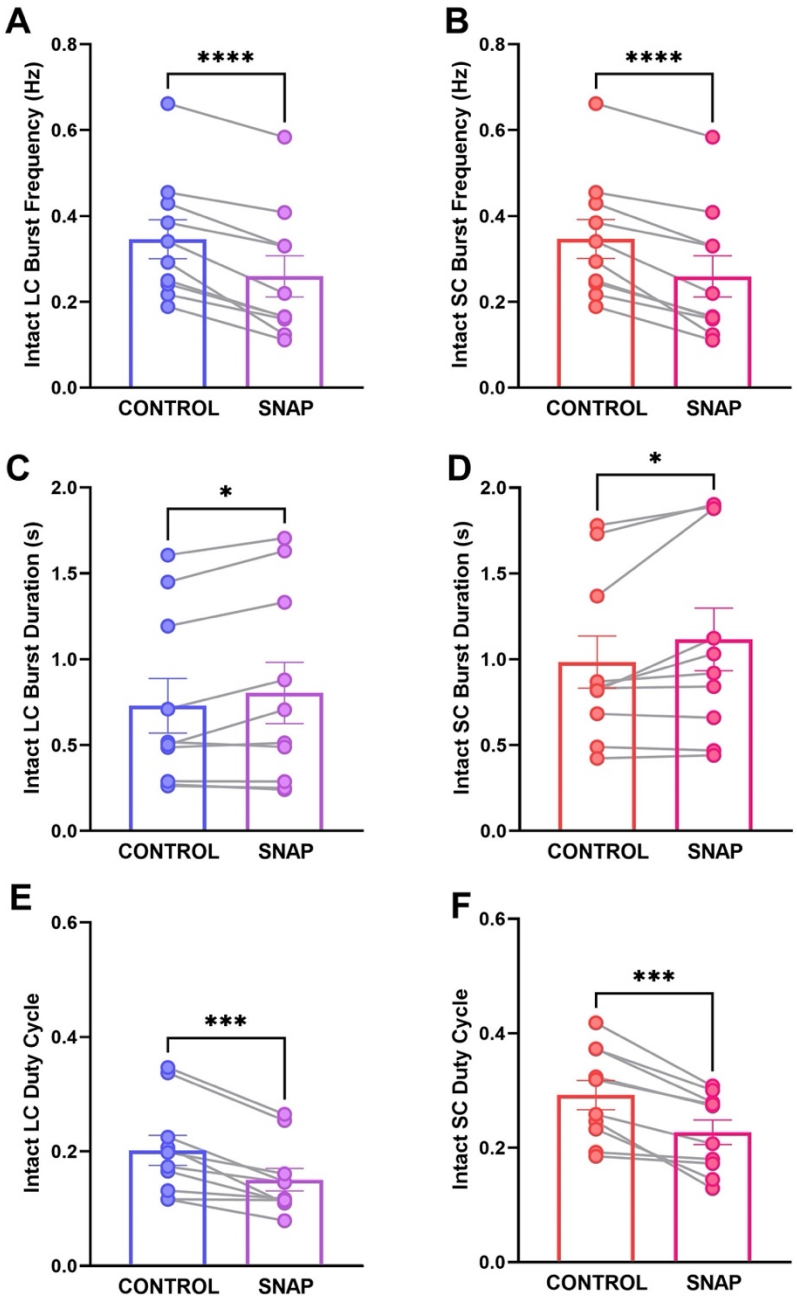

Figure 7. NO decreased the burst frequency and increased the burst duration of the intact CG. *(A and B)* In the intact CG, the coupled LCs and SCs significantly decreased in burst frequency after being perfused with 10^{-5} M SNAP ($p < 0.001$ for both cell types). *(C and D)* SNAP significantly increased the burst duration of the coupled LCs and SCs (LCs: $p = 0.0335$, SCs: $p = 0.0364$). *(E and F)* The duty cycle of both cell types significantly decreased in the presence of SNAP (LCs: $p = 0.0008$; SCs: $p = 0.0004$). Statistical significance was determined via paired two-tailed t-tests. Data presented as mean ± SEM. All conditions had a n=10. ** = $p < 0.01$, *** = $p < 0.001$.

3.3 NO differentially modulated the decoupled LCs and SCs.

Representative raw bursting traces of the ligatured LCs and SCs illustrated that SNAP elicited a decrease in the burst frequency of both cell types (Fig. 8A). The representative time course plots also suggested that SNAP decreased the burst frequency in the LCs and SCs (Fig. 8, B and C), though with a smaller effect on the SCs. The burst duration of both cell types increased in the presence of SNAP, but there was more burst-to-burst variability in the LCs. SNAP elicited a decrease in the SCs' duty cycle, an effect that was not shown in the time course graphs of the LCs.

In the ligatured preparations, SNAP significantly decreased the burst frequency of LCs but not SCs (paired two-tailed t-tests; LCs: $p = 0.005$, n = 10; SCs: $p = 0.2181$, n = 7; Fig. 9, A and B). Interestingly, SNAP had a bimodal effect on the SCs' burst frequency: several preparations increased in SCs' burst frequency, while several preparations decreased (Fig. 9B). The burst duration of the LCs did not significantly change in the presence of SNAP, while the SCs' burst duration significantly decreased (LCs: $p = 0.538$, n = 10; SCs: $p = 0.037$, n = 7; Fig. 9, C and D). Interestingly, several preparations had a decreased SCs' burst duration in response to SNAP, while several preparations with shorter burst durations were not affected. The ligatured LCs were trending towards a decrease in duty cycle when exposed to SNAP, while the ligatured SCs' duty cycle was significantly decreased (LCs: $p = 0.0702$, n = 10; SCs: $p = 0.018$, n = 7; Fig. 9, E and F). These results demonstrated that the bursting patterns of the LCs and SCs were differentially modulated by NO.

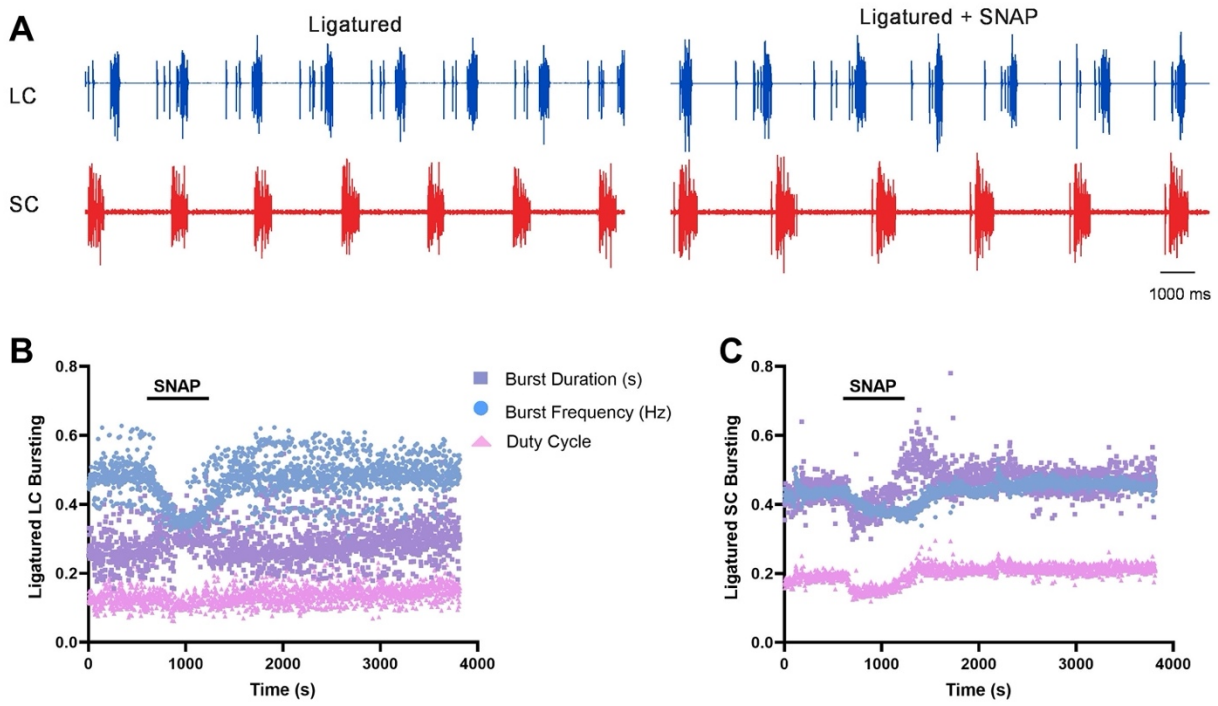

Figure 8. NO modulation of independent LCs and SCs in the ligatured CG. *(A)* Raw bursting traces of LCs (blue) and SCs (red) in a representative ligatured CG exposed to control saline and SNAP showed a decreased bursting frequency in both cell types, with a larger effect in the LCs. *(B)* In the ligatured preparations, SNAP decreased the burst frequency of LCs, while increasing the burst duration. The duty cycle was not shown to be affected by SNAP exposure. *(C)* While SNAP decreased burst frequency in the SCs to a smaller extent, the burst duration was increased more than the LCs. Additionally, there was a marginal decrease in the SCs duty cycle that was not seen in LCs. Ligatured preparations had greater variability in the bursting parameters compared to intact preparations.

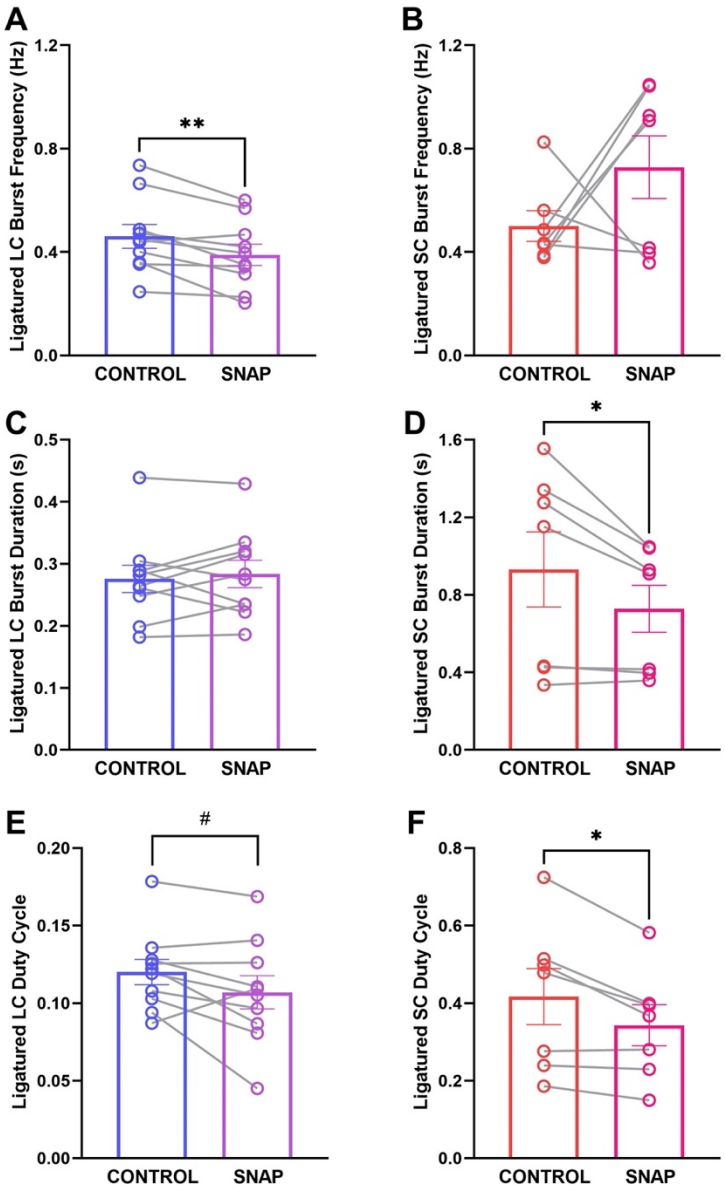

Figure 9. NO differentially modulated bursting of the LCs and SCs in the ligatured CG. *(A)* When decoupled by a ligature, the LCs' burst frequency decreased in SNAP ($p = 0.005$). *(B)* SNAP did not significantly affect the ligatured SCs' burst frequency when decoupled ($p = 0.2181$). Interestingly, SNAP had a bimodal effect on the burst frequency of ligatured SCs. *(C)* SNAP did not significantly affect the burst duration of ligatured LCs ($p = 0.538$). *(D)* However, SNAP significantly decreased the ligatured SCs' burst duration ($p = 0.0366$). *(E)* The ligatured LCs' duty cycle was trending towards a decrease in SNAP ($p = 0.070$). *(F)* The ligatured SCs' duty cycle was significantly decreased by SNAP ($p = 0.018$). Note that the y-axis range differs between the ligatured LCs and SCs to visualize the direction of change between control and SNAP conditions. Statistical significance was determined by paired two-tailed t-tests. Data presented as mean ± SEM. The ligatured SCs condition had a sample size of n=7, while all other conditions had a n=10. # = $p < 0.08$, * = $p < 0.05$, ** = $p < 0.01$.

3.4 The effects of NO on burst frequency and duration were state-dependent.

Given the variable responses to NO, I asked whether the effects of NO were state-dependent using two approaches. I first looked for state-dependent effects by analyzing the bursting in the SNAP condition as a function of the control condition, in relation to an identity line ($y = x$). A deviation from the identity line in a regular pattern would suggest state-dependent effects. Additionally, the preparations would lie along the graph's identity line if SNAP did not affect the bursting parameters. I also assessed for state-dependent effects by analyzing whether the baseline bursting parameters and the percent change from baseline had a direct or inverse relationship.

Comparing the burst frequencies in the control and SNAP conditions, the intact LCs' data points were consistently below the identity line, demonstrating that SNAP decreased the burst frequency (Fig. 10A). SNAP had a similar inhibitory effect on the SCs' burst frequency (Fig. 10B). There was no clear deviation from the line in the intact LCs or SCs, suggesting the effects of NO on the intact burst frequency were not state-dependent. In the ligatured LCs, several preparations had a decreased burst frequency in the presence of NO (Fig. 10C). The ligatured SCs varied in their responses to SNAP, with preparations increasing or decreasing in burst frequency (Fig. 10B). In the ligatured LCs and SCs, there was not a clear deviation from the identity line that suggested a frequency-dependent effect of NO. However, analyzing the percent change from baseline as a function of the baseline frequency revealed that SNAP inhibited the burst frequencies to a greater extent in the intact LCs and SCs starting with lower burst frequencies (Fig. 11, A and B). The frequency-dependent effects of NO were not seen in the percent change from baseline of the ligatured cell types (Fig. 11, C and D).

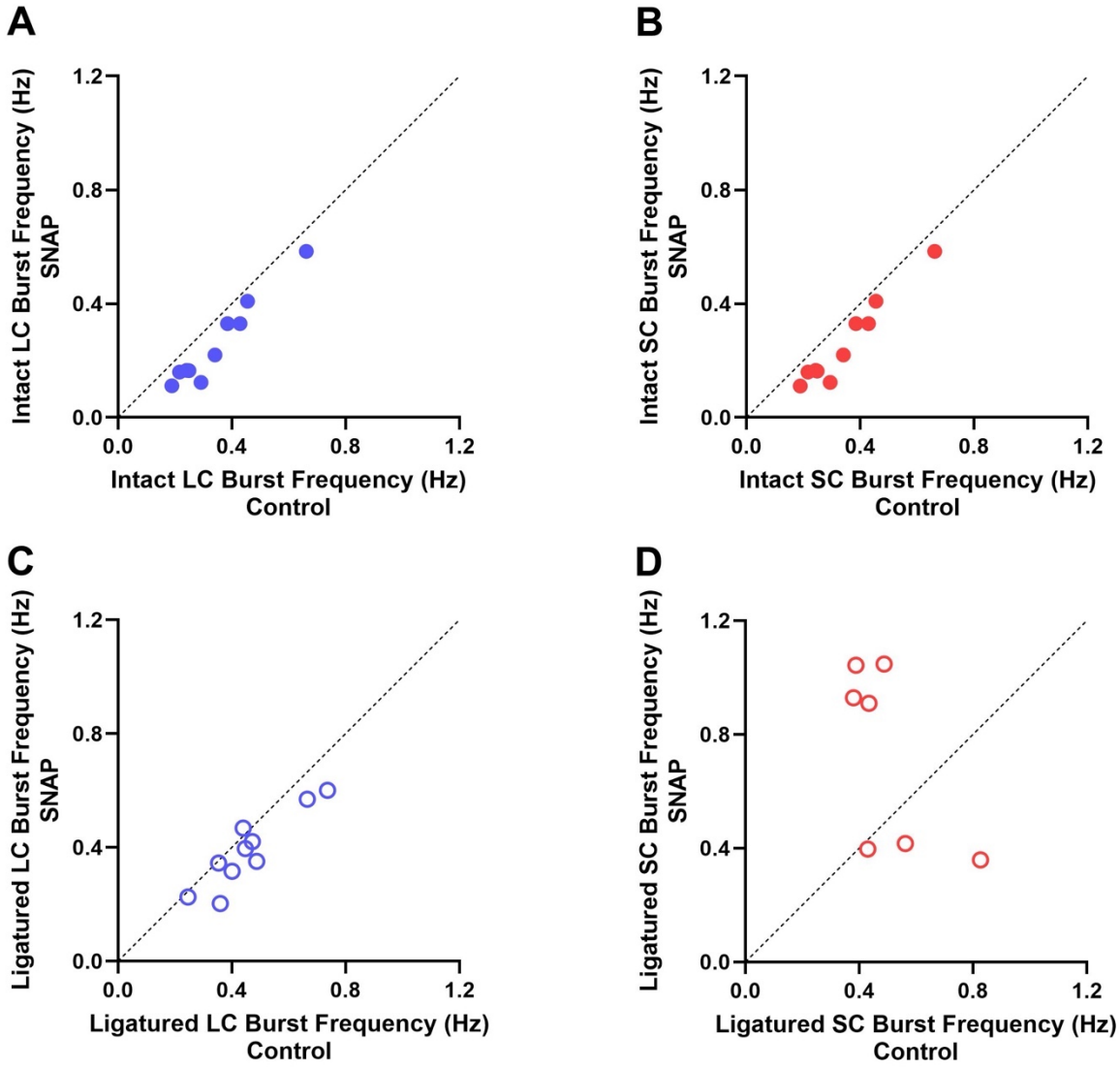

Figure 10. **Comparing the control and SNAP burst frequency demonstrated that the effects of NO were not clearly frequency-dependent.** The distribution of points in relation to the dotted identity line (y = x) demonstrated the effects of NO and whether the effects were state-dependent. *(A & B)* SNAP elicited a decrease in the burst frequency of the intact LCs and SCs in all samples. The decrease in burst frequency was relatively linear and did not indicate a frequency-dependent effect of NO. *(C)* SNAP decreased the burst frequency in the ligatured LCs in some samples and had a marginal effect in others. *(D)* In the ligatured SCs, there were two responses to SNAP. Some preparations had a large increase in burst frequency, while others decreased in frequency. There was no clear pattern of frequency-dependence in the ligatured LCs or SCs. The ligatured SCs had a n = 7, while all other conditions had a n=10.

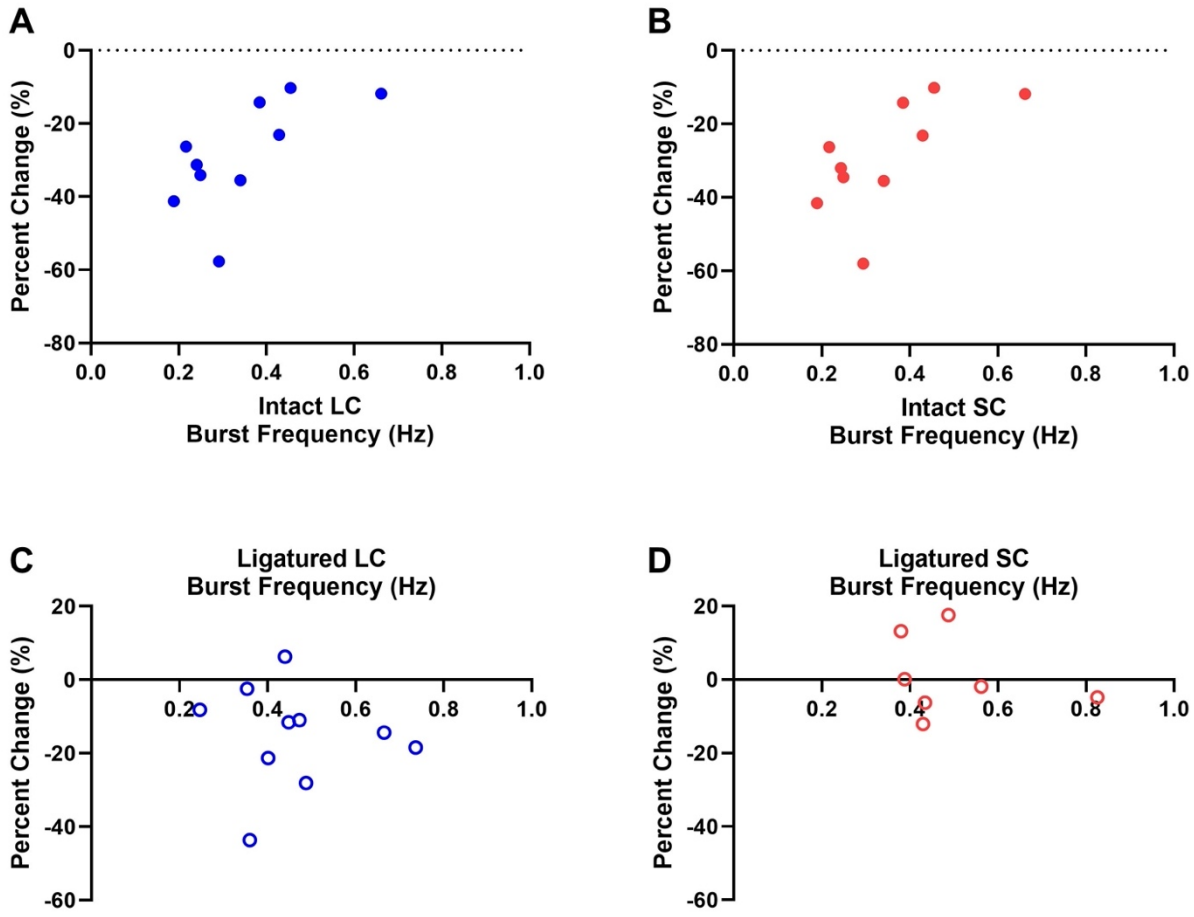

Figure 11. Percent change from baseline in burst frequency illustrated frequency-dependent effects of NO. *(A and B)* The inhibitory effects of NO were frequency-dependent in the intact LCs and SCs. SNAP elicited a larger decrease in the burst frequency of cells starting with lower burst frequencies. *(C and D)* There was no clear relationship between the percent change from baseline and the burst frequency of the ligatured LCs or SCs. SNAP decreased the burst frequency of many ligatured LCs to a greater extent than the ligatured SCs. Ligatured SCs had a n = 7, while all other conditions had a n=10. Note the y-axis difference between the intact and ligatured cell types.

While the burst durations of the intact LCs and SCs were increased by SNAP (Fig. 12, A and B), there were no clear patterns of deviation from the identity line. Thus, NO did not have state-dependent effects on the burst duration of intact LCs and SCs. The ligatured LCs also did not demonstrate clear effects of NO or state-dependent effects (Fig. 12C). Interestingly, the effects of NO on the ligatured SCs' burst duration were state-dependent. The SCs' burst duration in SNAP was increasingly inhibited as the baseline burst duration increased (Fig. 12D). SCs with a shorter baseline burst duration were not affected by SNAP, but cells with longer burst durations were affected. Analyzing the relationship between percent change and baseline burst duration also demonstrated that the effects of NO were state-dependent only in the ligatured SCs (Fig. 13). As the baseline burst duration of the SCs increased, there was a greater percent change from baseline. Thus, the effects of NO on burst frequency and duration were state-dependent in the LCs and SCs, illustrating the range of NO modulation across individual samples.

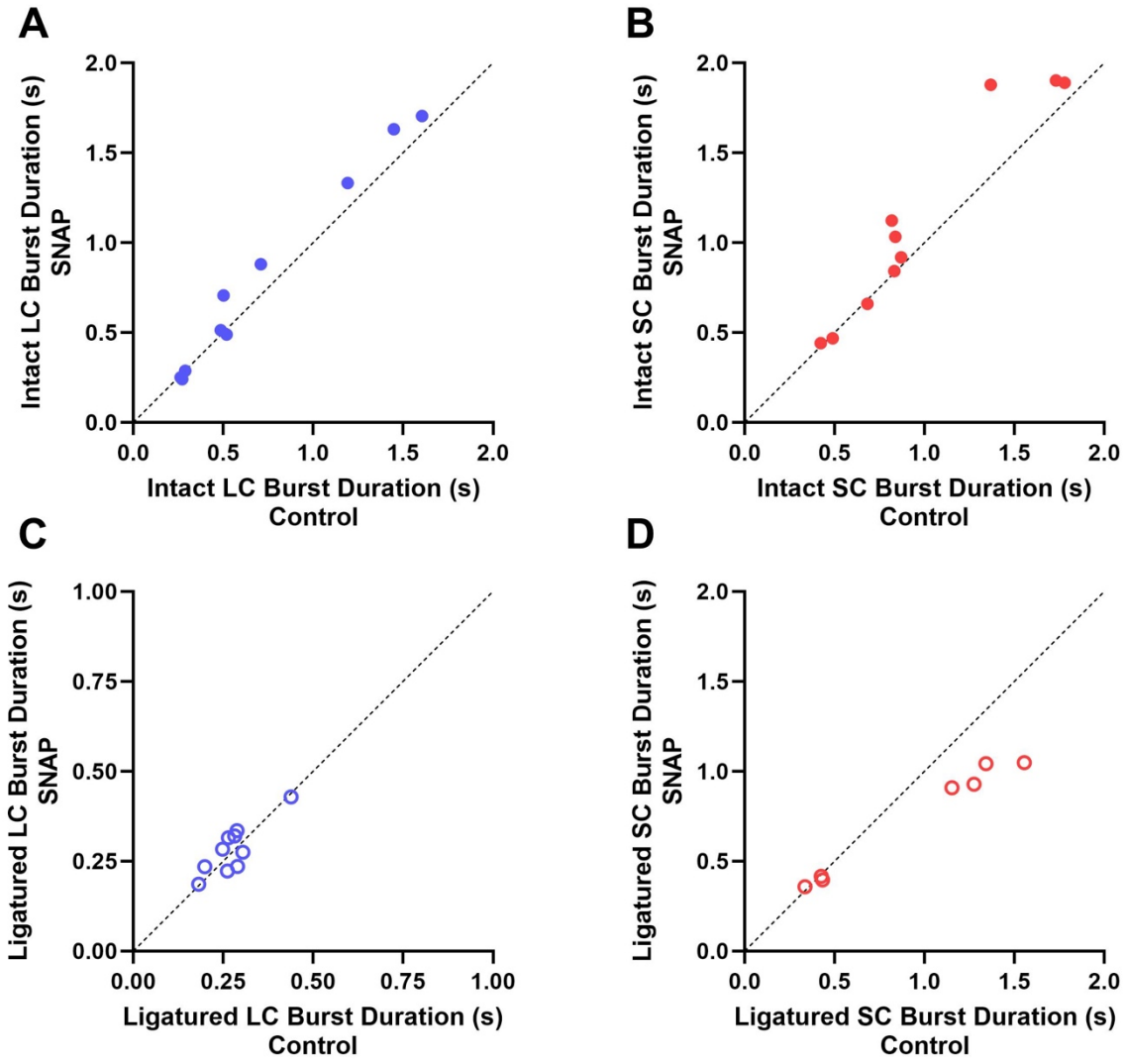

Figure 12. The effects of NO on the ligatured SCs' burst duration were state-dependent. The distribution of points in relation to the dotted identity line (y = x) demonstrated the effects of NO and whether the effects were state-dependent. *(A and B)* The burst duration of several intact LCs and SCs were increased by SNAP. There was no clear pattern of deviation from the identity line. *(C)* SNAP increased or decreased the ligatured LC's burst duration. The relationship between the burst duration in the control and SNAP condition of the ligatured LCs were relatively linear. *(D)* The burst duration of the ligatured SCs was increasingly inhibited by NO as the baseline burst duration increased. Ligatured SCs had a n = 7, while all other conditions had a n=10. Note the axis for the ligatured LCs burst duration differed from the other groups.

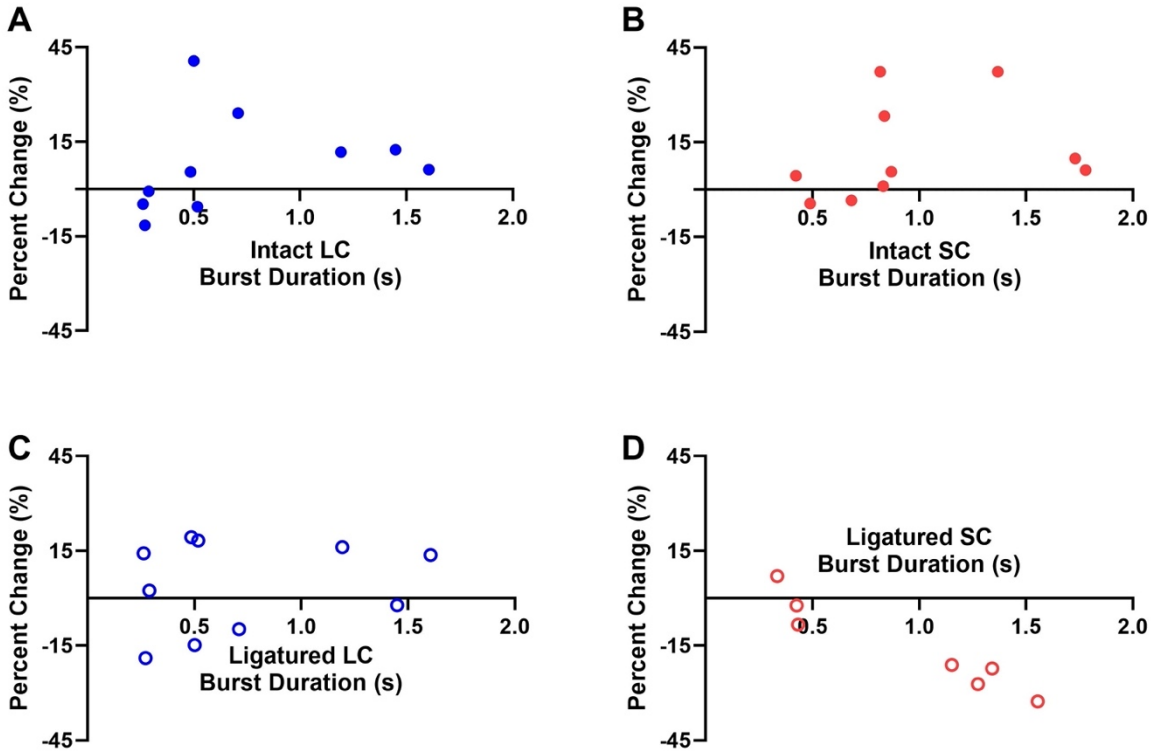

Figure 13. Percent change from baseline in burst duration demonstrate state-dependent effects of NO in the ligatured SCs. *(A & B)* There were no clear relationships between the percent change from baseline and the baseline burst duration in the intact CG. *(C)* SNAP had a range of effects on the ligatured LCs' burst duration, where the burst durations either increased or decreased. *(D)* The effects of NO on the SCs' burst duration were state-dependent. There was a greater percent change from baseline as the burst duration increased. Ligatured SCs had a n = 7, while all other conditions had a n=10.

3.5 NO increased the inactivation time constant of I_A rather than activation voltage-dependence.

TEVC was used to further understand the mechanisms of NO inhibition, specifically the modulation of the voltage-dependence of I_A activation and the current kinetics. Maximum peak outward current, peak I_A current, and I_A current inactivation were compared across control and SNAP conditions in an intact clamped LC1 or LC2. The protocol included a -90 mV step to maximally de-inactivate the I_A current before the sequence of increasing +10 mV steps. The I_A current was then determined by calculating the difference between the total peak outward current and steady state of each step.

The voltage-dependence of activation remained constant between the control and SNAP conditions (Fig. 14, A and B). Neither the total peak outward current nor the amplitude of the I_A current were significantly affected by SNAP at any voltage step (two-way mixed ANOVA, $p > 0.05$, n=4; Fig. 14, A and B). Interestingly, the time constant of I_A current inactivation did significantly increase (paired two-tailed t-test, $p = 0.0271$, n=4; Fig. 14C). Thus, NO alters the channel kinetics of the I_A current rather than the voltage-dependence of activation to elicit inhibition of bursting activity in the CG.

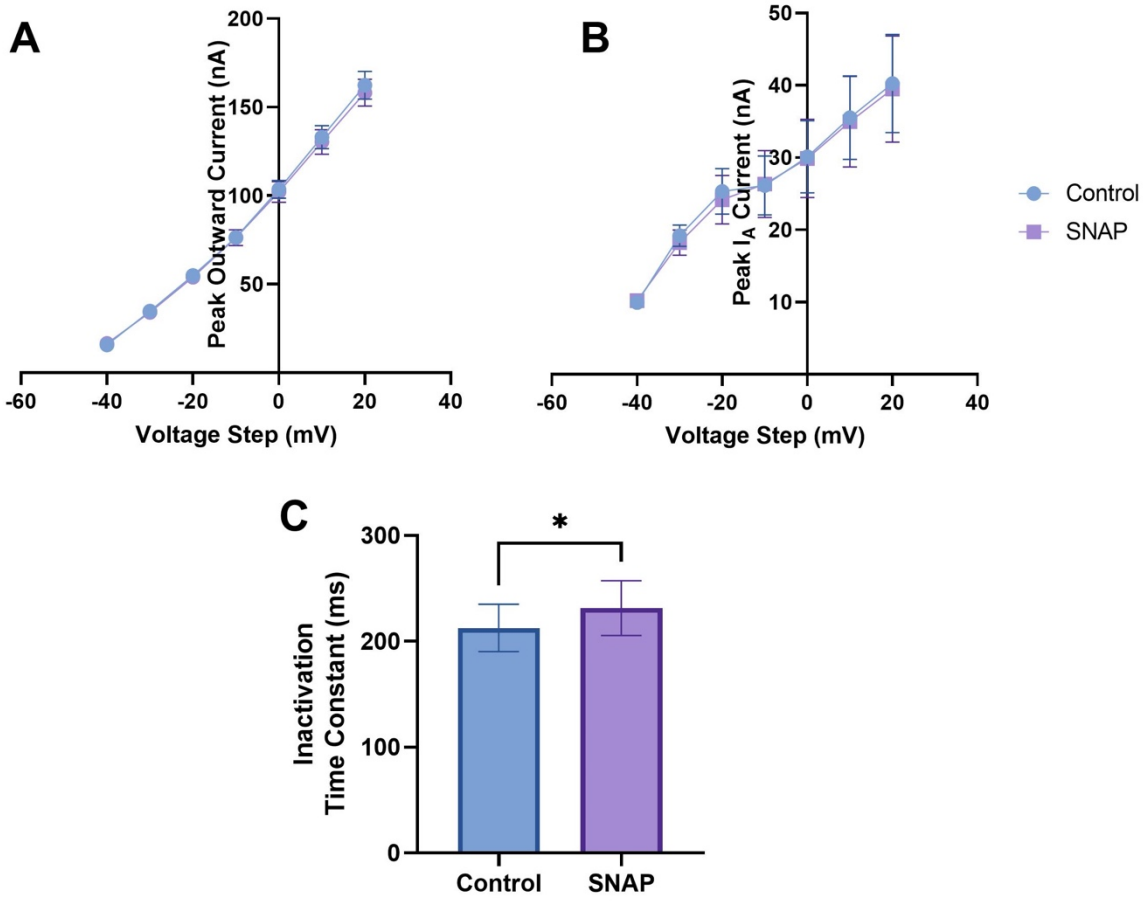

Figure 14. NO increased the I_A current inactivation time constant as measured by TEVC experiments. *(A & B)* SNAP did not significantly affect the peak outward current or peak I_A current across all voltage steps. The voltage-dependence of activation was not altered by SNAP. *(C)* Interestingly, SNAP increased the time constant of I_A current inactivation (two-tailed t-test, $p = 0.0271$). Peak current and time constants were determined using Spike2 analysis functions. Data presented as mean ± SEM. All conditions had n=4/group. * = $p < 0.05$.

4. Discussion

Investigating the mechanisms that elicit flexibility in the bursting patterns of the *Homarus* CG, a relatively simple 9-cell neural circuit, is critical for advancing our understanding of patterned movements and neural oscillators (Marder & Bucher, 2001; 2007). NO is a conserved endogenous neuromodulator among many organisms (Torreilles, 2001), so the mechanisms of NO intrinsic feedback may apply to many species. In humans, NO has many regulatory roles, such as modulating blood pressure via vasodilation (Cyr et al., 2020). While there are several differences between the neurogenic crustacean heart and the myogenic vertebrate heart, many of their currents are homologous (Tazaki & Cooke, 1986). Understanding the inhibitory effects of NO in the *Homarus* CG offers a foundational understanding of neuromodulation of CPGs.

In the negative feedback mechanism mediated by NO, it is known that increased heart muscle contractions release endogenously synthesized NO from the musculature (Mahadevan et al., 2004). As NO diffuses to the CG, the burst frequency decreases, which subsequently decreases the muscle contractions of the neurogenic crustacean heart (Mahadevan et al., 2004). While the feedback mechanism is well-characterized, the intracellular mechanisms by which NO modulates the CG are not well-known. Additionally, it has been shown that the LCs and SCs of the CG can be altered by neuromodulators in different manners (Oleisky et al., 2020). Thus, I sought to uncover whether NO modulates both cell types, whether there are different mechanisms of modulation between the cell types, and whether changes to the I_A current may be underlying NO modulation.

4.1 Overview of Results

In this study, my extracellular results confirmed that ligaturing the CG is effective in decoupling the cell types and establishing independent bursting patterns (Oleisky et al., 2020). Investigating SNAP's effects on the bursting parameters of the CG when intact and subsequently ligatured showed that NO decreased the duty cycle of both the LCs and the SCs by differentially modulating their bursting patterns. NO primarily decreased the ligatured LCs' burst frequency and SCs' burst duration to induce downstream inhibition of the cardiac musculature, supporting my hypothesis of different modulatory effects between cell types. Furthermore, I found that the effects of NO on the burst frequency and duration were state-dependent. My intracellular TEVC results showed that the inhibitory effects of NO are mediated by changes in the time constant of inactivation of the I_A current, among other possible molecular mechanisms, rather than the modulation of the voltage-dependence of I_A activation.

4.2 The functional implications of NO's effects on the intact CG.

My results demonstrated that NO inhibits the intact CG by decreasing the burst frequency and increasing the burst duration of the coupled LCs and SCs. Previous research has also shown that the CG burst frequency decreases when exposed to NO (Mahadevan et al., 2004). However, the increased burst duration of both the LCs and SCs in the intact CG elicited by NO was a novel finding highlighted by this study. The increased burst duration was a relatively small change compared to burst frequency. Additionally, this change was driven by a relatively large increase in only about half the preparations; burst duration remained unchanged in the other half of preparations. One possible mechanism underlying this change may be a decreased calcium sensitivity of the calcium-dependent potassium channels (I_{KCa}) elicited by NO. The build-up of

calcium in the cells activates the I_{KCa} channels, which rapidly hyperpolarize the cell and terminate the burst (Tazaki & Cooke, 1986; Cooke, 2002). Thus, a decreased calcium sensitivity of I_{KCa} channels would require greater levels of internal calcium to trigger the channels to open, resulting in a delayed hyperpolarization and increased burst duration. Future studies that analyze changes to I_{KCa} may further elucidate intracellular neuromodulation induced by NO.

Interestingly, NO's effects on the intact CG bursting activity are comparable with those of at least 2 other neuromodulators: allatostatin (AST) and myosuppressin. AST and myosuppressin are both highly conserved neuropeptides in invertebrates that also decrease burst frequency (Stemmler et al., 2007; Stevens et al., 2009; Szabo et al., 2011; Wiwatpanit et al., 2012; Oleisky et al., 2020). However, the effects of NO, AST, and myosuppressin on the CG lead to different functional implications on contraction amplitude.

The *Homarus* neuromuscular transform, a nonlinear mapping of neural signals to motor output, has shown that the CG burst frequency and duty cycle are correlated with the contraction amplitude (Williams et al., 2013). The effects of AST vary according to the animal, where a decreased burst frequency can produce either an increased or decreased contraction amplitude (Wiwatpanit et al., 2012). The increased contraction amplitude is elicited by the combination of a decrease in burst frequency and an even greater increase in burst duration, which results in an increased duty cycle. The decreased contraction amplitude is a function of a decreased burst frequency and constant burst duration, which results in a decreased duty cycle and decreased facilitation at the neuromuscular junction. The decreased contraction amplitude seen in AST is also mirrored in the downstream effects of NO (Mahadevan et al., 2004). Confirming previous findings (Mahadevan et al., 2004), my results suggest that the decreased amplitude is mediated by

a decreased burst frequency and a relatively small increase in burst duration that results in a decreased duty cycle.

Myosuppressin also decreases the burst frequency and duty cycle of the CG, but it additionally modulates the peripheral muscles, leading to different effects on the contraction amplitude (Stevens et al., 2009). While the neuromuscular transform would predict that the decreased CG duty cycle would result in a decreased amplitude (Williams et al., 2013), the peripheral effects of myosuppressin cause a large increase in amplitude (Stevens et al., 2009). The central effect of myosuppressin in its nonamidated form on the CG decreases the amplitude (Oleisky et al., 2020), but this decrease is masked by the increased amplitude elicited by the peripheral muscles (Stevens et al., 2009).

Of the neuromodulators that have been found to decrease the burst frequency and duty cycle of the CG, NO is the only one that elicits a singular effect on the contraction amplitude. The neuromuscular transform predicts the effects of NO with the highest accuracy because of the clear relationship between the decreased duty cycle and subsequently decreased contraction amplitude. My results confirmed that NO decreases the burst frequency of the LCs and SCs in the intact CG, while also demonstrating that NO increases the burst duration. NO elicits effects in the CG similar to other neuromodulators, but NO has different functional implications.

4.3 NO differentially modulated the LCs and SCs to decrease the duty cycle.

From analyzing the bursting activity of the decoupled LCs and SCs, my results demonstrated that NO inhibits the LCs' burst frequency, while inducing a bimodal effect on the SCs. The different responses of the two cell types suggest that NO inhibited the LC's burst frequency independently of the SCs in the decoupled preparation. The inhibitory effect of NO in

the LCs mirrored the decreased burst frequency when the cells were coupled, suggesting that NO mediates a negative feedback mechanism within the CG by acting predominantly on the LCs. Since the crustacean heart is entirely neurogenic, changes to the heart contraction frequency will mirror changes to the LCs' burst frequency. According to the neuromuscular transform, changes to the duty cycle and frequency will likely be reflected in the heartbeat amplitude (Williams et al., 2013). The decreased burst frequency of LCs will directly inhibit the heart contraction frequency and, assuming there are not significant changes in the burst duration, indirectly decrease the heartbeat amplitude. Given the consistent, large changes in the LCs' burst frequency and the variable effects in SCs, this finding strongly suggests different mechanisms of modulation between the cell types.

Interestingly, NO elicited contrasting effects on the LCs' and SCs' burst duration between the intact and ligatured preparation. In intact preparations, NO increased the burst duration of both cell types. Since there was no effect of NO on the ligatured LCs, the increased LCs' burst duration in the intact CG was likely due to the electrical and chemical coupling to the SCs (Hartline 1979; Cooke, 2002). An increased burst duration increases the refractory period and subsequently decreases the bursting frequency (Tazaki & Cooke, 1990). In the intact CG, the increased burst duration of both cells may be driving the decreased burst frequency, in addition to the independent effects of NO on the LCs.

In the ligatured preparations, NO significantly decreased the SCs' burst duration, while the LCs' burst duration was not altered. The decreased SCs' burst duration may be mediated by an increased calcium sensitivity in these cells, such that the I_{KCa} channels open at lower levels of calcium in the cell. The activation of these potassium channels will rapidly hyperpolarize the cell and end the burst (Tazaki & Cooke 1986; Cooke, 2002). The different effects of NO on the burst duration between the intact and ligatured SCs may be mediated by the coupling between the intact

LCs and SCs, though the mechanisms that result in an increased duration in the intact CG are not clear.

The effects of NO on the bursting characteristics of the ligatured preparations suggest that LCs have greater control in determining the burst frequency, while the SCs are more significant for eliciting changes in burst duration. These distinct roles of the LCs and SCs are also seen in the effects of myosuppressin in the ligatured CG (Oleisky et al., 2020). The different modulatory effects of NO on the LCs and SCs allow for varying degrees of inhibitory feedback and robust neuromodulation of the CG.

4.4 The effects of NO on burst frequency and duration were state-dependent.

There were variable effects of NO on the CG bursting patterns, perhaps mediated by animal-to-animal differences in the modulatory mechanisms responding to varying levels of endogenous NO production (Mahadevan et al., 2004). To further characterize NO modulation, I investigated whether the effects were state-dependent. Modulation is state-dependent in several systems; for instance, the neuropeptide proctolin increases the burst frequency of the crustacean stomatogastric ganglion when the baseline frequency is low, but it does not modulate high baseline frequencies (Hooper & Marder 1987; Nusbaum & Marder, 1989). AST oppositely modulates the crab stomatogastric ganglion, such that there is increased inhibition of starting frequencies slower than 0.8 Hz and little effect on faster frequencies (Skiebe & Schneider, 1994). Additionally, the non-linear lobster cardiac neuromuscular transform accurately predicts the state-dependent neuromodulation of AST (Williams et al., 2013). Given the abundance of state-dependent modulation in the crustacean heart, I asked whether the effects of NO were also state-dependent.

Since lower burst frequencies would suggest smaller average total conductance, I expected a muted effect of NO at higher frequencies. A smaller conductance is reflective of high resistance, so currents modulated by NO at a lower bursting frequency would likely have a greater change. My results suggest that the effects of NO were frequency-dependent in the intact LCs and SCs with a larger effect on lower burst frequencies. Interestingly, the frequency-dependence was demonstrated when analyzing the percent change from baseline, but it was not clearly seen when directly comparing the burst frequency of control and SNAP conditions. This discrepancy may be explained by the limited range of burst frequencies within my samples (predominately 0.2-0.4 Hz) or a potential floor effect. The frequency-dependent effects of NO may be masked at lower frequencies to maintain rhythmic bursting in the CG. Expanding the sample to include an increased range of baseline burst frequencies may confirm the frequency-dependent effects of NO.

My results also revealed that the effects of NO were duration-dependent in the ligatured SCs. The state-dependent effects of NO on the SCs' burst duration may support biological functioning, such that NO does not further down-regulate and inhibit shorter burst durations to maintain overall bursting. Decreasing the burst duration when already short may dysregulate rhythmic bursting, possibly leading to tonic firing. Modeling studies have shown that the baseline variability changes a preparation's position in the conductance space, a theoretical map of conductance values, based on the distribution and number of channels (Marder et al., 2014). The position within the conductance map, dictated by the several underlying conductance values, influences the extent of neuromodulation (Marder et al., 2014).

The variability of NO's effects between preparations and between cell types may also be explained by different intracellular targets of NO-cGMP signaling. Increased levels of NO activate NO-dependent guanylate cyclase (Scholz et al., 2002; Bicker 2007), which converts GTP to cyclic

GMP (cGMP). The production of cGMP may activate cGMP-dependent protein kinases that modulate a variety of targets, such as transcription factors and ion channels. For instance, NO has been implicated in a slower mechanism of transcriptional modulation by altering the target of rapamycin (TOR) signaling pathway to mediate the effects of the crustacean molt-inhibiting hormone (Soliman, 2005; Mykles & Chang, 2020). The modulation of ion channels in the CG, such as the I_A channel, is a more probable target mediating the changes to bursting since the effects of NO have a faster time course. Future studies that analyze the levels and targets of active cGMP in the LCs and SCs may further reveal the mechanisms underlying the range of NO neuromodulation in the CG. There are several possible mechanisms that contribute to the state-dependent effects of NO, which can facilitate unique neuromodulation that appropriately responds to the intrinsic biological variability.

4.5 NO increased the inactivation time constant of I_A currents.

The bursting patterns of neurons can be altered by several changes in currents, such as the voltage-dependence of activation or the channel kinetics for inactivation (Harris-Warrick & Marder, 1991; Marder & Calabrese, 1996; Dickinson, 2006). Modulation of the voltage-dependence of activation can be determined by measuring the peak current as a function of voltage, while the modulation of channel kinetics is often reflected by changes to the time-dependence of activation or inactivation. I hypothesized that NO modulation was mediated by an increased I_A current that increased hyperpolarization of the cell. The increase in I_A current could be mediated by an altered maximum conductance, voltage-dependence of activation, or time constant of inactivation. Synaptic excitation of the cell depolarizes the cell, but an increased I_A current induced by NO slows the depolarization to reach the firing threshold for the

next driver potential (Cooke, 2002). Additionally, the I_A current has been theorized to be key for phase consistency for a rhythmic network in modeling studies (Greenberg & Manor, 2005). In the LCs, the I_A current mediates compensatory plasticity to restore excitability in the crustacean cardiac ganglion (Schulz & Lane, 2017). Thus, the I_A current is vital for rhythmic bursting and may be modulated by NO to elicit inhibited bursting activity.

Intracellular TEVC recordings from one of the LCs demonstrated that neither the total peak outward current nor the peak I_A current was altered by NO at any voltage step. These results suggest that the voltage-dependence of activation and maximum current amplitude were not responsible for mediating the changes in burst frequency elicited by NO. The TEVC recordings did demonstrate that NO modulates channel kinetics, specifically by increasing the time constant of inactivation. This change could underlie the decreased burst frequency in the LCs. An increased time constant of inactivation would indicate that the I_A channels close at a slower exponential rate, allowing the cell to be hyperpolarized for longer period (Tazaki & Cooke, 1986; Cooke, 2002). The slower inactivation of the I_A current would decrease the depolarization to the bursting threshold and decrease the burst frequency of the cell. These findings suggest that NO modulates the time-dependence of I_A current inactivation among other changes to channel kinetics, rather than its voltage-dependence of activation.

5. Conclusion

In this thesis, I have explored the mechanisms of NO neuromodulation of the lobster cardiac ganglion. I investigated the effects of NO on two neurophysiological levels: the extracellular bursting activity and the intracellular voltage-dependence of activation and time constant of inactivation. NO inhibited the CG by differentially modulating the bursting activity of the two cell types. NO decreased the burst frequency of the LCs while decreasing the burst duration of the SCs. The effects of NO on the SCs' burst duration were also state-dependent, which may underlie robust neuromodulation of the CG. Additionally, NO modulated the time constant of inactivation of the I_A current, which is one possible mechanism that may have decreased the LCs' burst frequency. This project has further characterized the negative feedback mechanism of NO and the intracellular mechanisms critical for maintaining rhythmicity in CPG networks.

6. References

Berlind, A. (1989). Feedback from motor neurones to pacemaker neurones in lobster cardiac ganglion contributes to regulation of burst frequency. *Journal of Experimental Biology*, *141*(1), 277-294.

Bicker G. (2007). Pharmacological approaches to nitric oxide signalling during neural development of locusts and other model insects. *Archives of Insect Biochemistry and Physiology*, *64*(1), 43–58.

Cooke, I. M. (2002). Reliable, responsive pacemaking and pattern generation with minimal cell numbers: The crustacean cardiac ganglion. *The Biological Bulletin, 202*(2), 108-136.

Christie, A. E., Hull, J. J., & Dickinson, P. S. (2020). In silico analyses suggest the cardiac ganglion of the lobster, Homarus americanus, contains a diverse array of putative innexin/innexin-like proteins, including both known and novel members of this protein family. *Invertebrate Neuroscience, 20*(2), 5.

Cyr, A. R., Huckaby, L. V., Shiva, S. S., & Zuckerbraun, B. S. (2020). Nitric Oxide and Endothelial Dysfunction. *Critical Care Clinics*, *36*(2), 307–321.

Dickinson, P. S. (2006). Neuromodulation of central pattern generators in invertebrates and vertebrates. *Current Opinion in Neurobiology, 16*(6), 604-614.

Greenberg, I., & Manor, Y. (2005). Synaptic depression in conjunction with A-current channels promote phase constancy in a rhythmic network. *Journal of Neurophysiology*, *93*(2), 656-677.

Klinger, J. R., & Kadowitz, P. J. (2017). The Nitric Oxide Pathway in Pulmonary Vascular Disease. *The American Journal of Cardiology*, *120*(8S), S71–S79.

Harris-Warrick, R. M., & Marder, E. (1991). Modulation of Neural Networks for Behavior. *Annual Review of Neuroscience, 14*(1), 39-57.

Hartline, D. K. (1967). Impulse identification and axon mapping of the nine neurons in the cardiac ganglion of the lobster Homarus americanus. *Journal of Experimental Biology*, *47*(2), 327-341.

Hartline, D. K. (1979). Integrative Neurophysiology of the Lobster Cardiac Ganglion. *American Zoologist, 19*(1), 53-65.

Hooper, S. L., & Marder, E. (1987). Modulation of the lobster pyloric rhythm by the peptide proctolin. *The Journal of* Neuroscience, *7*(7), 2097–2112.

Hooper, S. L., & DiCaprio, R. A. (2004). Crustacean Motor Pattern Generator Networks. *Neurosignals, 13*(1-2), 50-69.

Hooper, S. L., Thuma, J. B., Guschlbauer, C., Schmidt, J., & Büschges, A. (2015). Cell dialysis by sharp electrodes can cause nonphysiological changes in neuron properties. *Journal of Neurophysiology, 114*(2), 1255-1271.

Mahadevan, A., Lappé, J., Rhyne, R. T., Cruz-Bermúdez, N. D., Marder, E., & Goy, M. F. (2004). Nitric oxide inhibits the rate and strength of cardiac contractions in the lobster Homarus americanus by acting on the cardiac ganglion. *The Journal of Neuroscience*, *24*(11), 2813–2824.

Marder, E. & Calabrese, R. L. (1996). Principles of rhythmic motor pattern generation. *Physiological Reviews*, *76*(3), 687–717.

Marder, E., & Bucher, D. (2001). Central pattern generators and the control of rhythmic movements. *Current Biology, 11*(23), R986-R996.

Marder, E., & Bucher, D. (2007). Understanding Circuit Dynamics Using the Stomatogastric Nervous System of Lobsters and Crabs. *Annual Review of Physiology, 69*(1), 291-316.

Marder, E., O'Leary, T., & Shruti, S. (2014). Neuromodulation of circuits with variable parameters: single neurons and small circuits reveal principles of state-dependent and robust neuromodulation. *Annual Review of Neuroscience*, *37*, 329–346.

Mykles, D. L., & Chang, E. S. (2020). Hormonal control of the crustacean molting gland: Insights from transcriptomics and proteomics. *General and Comparative Endocrinology*, *294*, 113493.

Nusbaum, M. P., & Marder, E. (1989). A modulatory proctolin-containing neuron (MPN). II. State-dependent modulation of rhythmic motor activity. *The Journal of Neuroscience*, *9*(5), 1600–1607.

Oláh, G., Módis, K., Törö, G., Hellmich, M. R., Szczesny, B., & Szabo, C. (2018). Role of endogenous and exogenous nitric oxide, carbon monoxide and hydrogen sulfide in HCT116 colon cancer cell proliferation. *Biochemical Pharmacology*, *149*, 186–204.

Oleisky, E. R., Stanhope, M. E., Hull, J. J., Christie, A. E., & Dickinson, P. S. (2020). Differential neuropeptide modulation of premotor and motor neurons in the lobster cardiac ganglion. *Journal of Neurophysiology*, *124*(4), 1241–1256.

Scholz, N. L., Labenia, J. S., de Vente, J., Graubard, K., & Goy, M. F. (2002). Expression of nitric oxide synthase and nitric oxide-sensitive guanylate cyclase in the crustacean cardiac ganglion. *The Journal of Comparative Neurology*, *454*(2), 158–167.

Schulz, D. J., & Lane, B. J. (2017). Homeostatic plasticity of excitability in crustacean central pattern generator networks. *Current Opinion in Neurobiology, 43*, 7-14.

Skiebe, P., & Schneider, H. (1994). Allatostatin peptides in the crab stomatogastric nervous system: inhibition of the pyloric motor pattern and distribution of allatostatin-like immunoreactivity. *Journal of Experimental Biology*, *194*, 195–208.

Soliman G. A. (2005). The mammalian target of rapamycin signaling network and gene regulation. *Current Opinion in Lipidology*, *16*(3), 317–323.

Stemmler, E. A., Cashman, C. R., Messinger, D. I., Gardner, N. P., Dickinson, P. S., & Christie, A. E. (2007). High-mass-resolution direct-tissue MALDI-FTMS reveals broad conservation of three neuropeptides (APSGFLGMRamide, GYRKPPFNGSIFamide and pQDLDHVFLRFamide) across members of seven decapod crustaean infraorders. *Peptides*, *28*(11), 2104–2115.

Stevens, J. S., Cashman, C. R., Smith, C. M., Beale, K. M., Towle, D. W., Christie, A. E., & Dickinson, P. S. (2009). The peptide hormone pQDLDHVFLRFamide (crustacean myosuppressin) modulates the Homarus americanus cardiac neuromuscular system at multiple sites. *Journal of Experimental Biology*, *212*(24), 3961–3976.

Szabo, T. M., Chen, R., Goeritz, M. L., Maloney, R. T., Tang, L. S., Li, L., & Marder, E. (2011). Distribution and physiological effects of B-type allatostatins (myoinhibitory peptides, MIPs) in the stomatogastric nervous system of the crab Cancer borealis. *The Journal of Comparative Neurology*, *519*(13), 2658–2676.

Tazaki, K., & Cooke, I. M. (1986). Currents under voltage clamp of burst-forming neurons of the cardiac ganglion of the lobster (Homarus americanus). *Journal of Neurophysiology*, *56*(6), 1739–1762.

Tazaki, K.; Cooke, I. M. (1990). Characterization of Ca current underlying burst formation in lobster cardiac ganglion motor neurons. *Journal of Neurophysiology, 63(2),* 370–384.

Tenopoulou, M., & Doulias, P. T. (2020). Endothelial nitric oxide synthase-derived nitric oxide in the regulation of metabolism. *F1000Research*, *9*, F1000 Faculty Rev-1190.

Torreilles J. (2001). Nitric oxide: one of the more conserved and widespread signaling molecules. *Frontiers in Bioscience*, *6*, D1161–D1172.

Totzeck, M., Hendgen-Cotta, U. B., & Rassaf, T. (2017). Nitrite-Nitric Oxide Signaling and Cardioprotection. *Advances in Experimental Medicine and Biology*, *982*, 335–346.

Tse J. (2017). Gut Microbiota, Nitric Oxide, and Microglia as Prerequisites for Neurodegenerative Disorders. *ACS chemical neuroscience*, *8*(7), 1438–1447.

Williams, A. H., Calkins, A., O'Leary, T., Symonds, R., Marder, E., & Dickinson, P. S. (2013). The Neuromuscular Transform of the Lobster Cardiac System Explains the Opposing Effects of a Neuromodulator on Muscle Output. *The Journal of Neuroscience, 33*(42), 16565-16575.

Wiwatpanit, T., Powers, B., & Dickinson, P. S. (2012). Inter-animal variability in the effects of C-type allatostatin on the cardiac neuromuscular system in the lobster Homarus americanus. *The Journal of Experimental Biology*, *215*(13), 2308–2318.

Yamakawa, T., Kurauchi, Y., Hisatsune, A., Seki, T., & Katsuki, H. (2018). Endogenous Nitric Oxide Inhibits, Whereas Awakening Stimuli Increase, the Activity of a Subset of Orexin Neurons. *Biological & Pharmaceutical Bulletin*, *41*(12), 1859–1865.

Zhang Y. H. (2017). Nitric oxide signalling and neuronal nitric oxide synthase in the heart under stress. *F1000Research*, *6*, 742.